LLNL-JRNL-2003812

Lawrence Livermore National Laboratory

Neutron capture signatures inferred from gadolinium isotope compositions of uranium ore concentrates

J Render, G Brennecka, A Herbst, Q Shollenberger, A Johnson

June 2025

Disclaimer

This work performed under the auspices of the U.S. Department of Energy by Lawrence Livermore National Laboratory under Contract DE-AC52-07NA27344.

Title page

Names of the authors: Quinn R. Shollenberger[*], Ashley K. Herbst[a], Adelicia F. Johnson[b], Jan Render, Gregory A. Brennecka

Title: Neutron capture signatures determined from gadolinium isotope compositions of uranium ore concentrates using MC-ICPMS

Affiliation(s) and address(es) of the author(s):

Nuclear & Chemical Sciences Division, Lawrence Livermore National Laboratory, 7000 East Avenue L-231, Livermore, CA 94550 USA.

[a]present address: School of Earth and Space Exploration, Arizona State University, P.O. Box 871404, Tempe, AZ 85287-1404, USA.

[b]present address: Ocean Sciences Department, Univeristy of California, Santa Cruz, 1156 High Street, Santa Cruz, CA 95064, USA.

*E-mail address of the corresponding author: shollenberger@llnl.gov

This study was designed by Gregory Brennecka and Quinn Shollenberger. Material preparation, data collection and analysis were performed by all authors. The first draft of the manuscript was written by Quinn Shollenberger and all authors commented on previous versions of the manuscript. All authors read and approved the final manuscript.

Neutron capture signatures determined from gadolinium isotope compositions of uranium ore concentrates using MC-ICPMS

Quinn R. Shollenberger[1], Ashley K. Herbst[1], Adelicia F. Johnson[1], Jan Render[1], Gregory A. Brennecka[1]

[1]*Nuclear & Chemical Sciences Division, Lawrence Livermore National Laboratory, 7000 East Avenue L-231, 94550 Livermore, USA*

Abstract

We present Gd isotope compositions on 25 well-characterized uranium ore concentrates (UOCs). About half the UOCs have isotope depletions in ^{157}Gd coupled with anticorrelated excesses in ^{158}Gd due to neutron capture effects. UOCs from older ore bodies and with higher U contents show larger neutron capture effects than UOCs from younger ore bodies with lower U contents. These data, along with previously measured Sm isotope compositions, are used to estimate the neutron fluence and energy spectrum of these samples, demonstrating how combined Sm and Gd signatures could be employed as a new tool for nuclear forensics.

Keywords

nuclear forensics, origin assessment, gadolinium isotopes, uranium ore concentrate, thermal neutron capture

Article highlights

- Neutron capture effects are measurable in Gd isotopes of UOCs from older U deposits
- Sm and Gd isotopes used to estimate neutron fluence and energy spectrum of the UOCs
- Gd isotopes are a new tool to support nuclear forensics investigations

1. Introduction

Nuclear material found outside of regulatory control is a concern to law enforcement and other governmental agencies worldwide. When this happens, nuclear forensic science, also known informally as nuclear forensics, can be used to help answer investigative questions like: When and where did the material fall out of regulatory control? Where did the material originate? Is there likely to be more of that material? These questions can be addressed utilizing nuclear forensic signatures or material characteristics that allow the provenance and history of a sample to be determined [1-2].

One specific material of concern that is commonly traded on the worldwide market is uranium ore concentrate (UOC), also known as yellowcake [3]. Nuclear forensics signatures that are typically employed to determine the origin and history of interdicted UOC include U isotope compositions [4-5], $^{87}Sr/^{86}Sr$ isotope compositions [6-7], $^{143}Nd/^{144}Nd$ isotope compositions [8-9], Pb isotope compositions [6-7], as well as major and trace element abundances [5, 7, 10-13]. Variations in the isotope compositions and trace element abundances can be caused by different processes and can inform about the history and provenance of the UOC. For example, variations in $^{238}U/^{235}U$ as well as in Mo and Re isotope ratios can be caused by mass-dependent isotope

63 fractionation or nuclear volume effect and provide information on the physical processes
64 connected to the original U ore body but can also be affected during UOC production [4, 14-15].
65 On the other hand, variations in Pb isotope systematics, $^{87}Sr/^{86}Sr$, $^{143}Nd/^{144}Nd$, and $^{234}U/^{235}U$ are
66 radiogenic in nature and are indicative of the geologic sources of the original ore body.
67 Importantly, it has been shown that some signatures like $^{87}Sr/^{86}Sr$, Pb isotopes, and elemental
68 abundances are less reliable because they can be altered by the processing steps used to produce
69 UOC [6-7]. More recently, [16] demonstrated the use of mass-independent ^{149}Sm and ^{150}Sm
70 isotope variations in determining the original uranium ore body type from which the UOC is
71 derived. One benefit to using Sm isotopes as a nuclear forensics signature is that Sm is rare in the
72 industrial environments and processes associated with UOC production. Furthermore, these Sm
73 isotope variations in UOCs are not caused by mass-dependent fractionation processes or
74 radiogenic effects but instead reflect the neutron irradiation history of a particular ore body.
75 Layering such fundamentally different nuclear forensic signatures together provides the highest
76 confidence in determining the origin of material found outside of regulatory control.

77 The use of Sm isotopes as a signature in nuclear forensics stems from its intrinsic
78 property of having an isotope (^{149}Sm) with a large thermal neutron capture cross section
79 (~40,000 barns; [17]). This means that a thermalized neutron can be captured within a uranium
80 ore body by ^{149}Sm transmuting into ^{150}Sm. Neutrons within a uranium ore body come from the
81 spontaneous fission of ^{238}U, neutron-induced fission of ^{235}U, and (α,n) reactions. [16] found that
82 UOCs derived from older ore bodies (~>1.5Ga) with higher U contents were more likely to
83 display measurable Sm isotope variations. Conversely, UOCs derived from younger ore bodies
84 with lower U contents did not show measurable Sm isotope variations. Another rare earth
85 element (REE), gadolinium (Gd), has two isotopes with even larger thermal neutron capture

86 cross sections than ^{149}Sm: ^{155}Gd (60,900 barns) and ^{157}Gd (254,000 barns) [17], meaning they are
87 even more likely to capture thermalized neutrons compared to ^{149}Sm. The large thermal neutron
88 capture cross sections of Gd isotopes, combined with the low background of Gd in nuclear
89 industry environments and within reagents used to process UOCs makes Gd an ideal candidate
90 element for nuclear forensics. The low background of Gd during UOC production means that it
91 is less susceptible to contamination and therefore reflects the Gd isotope composition of the
92 original U ore body. Furthermore, Sm and Gd signatures can be used to quantify the neutron
93 fluence within an ore body [18-19], potentially providing even more information on the
94 provenance of an unknown sample. However, while some Gd isotope composition data have
95 been reported for U ores [18-19], they have not been measured in UOCs.

96 Previous studies have used thermal ionization mass spectrometry (TIMS) to measure Gd
97 isotope compositions in both terrestrial and extraterrestrial rocks [*e.g.,* 19-21]. However, TIMS
98 has a relatively low ionization efficiency for Gd^+ which effectively requires more sample
99 material and has a slower sample throughput compared to a multi-collector inductively coupled
100 plasma mass spectrometer (MC-ICPMS). Although Gd isotope ratios can be measured via TIMS
101 as GdO^+ rather than Gd^+ to increase ionization efficiency, issues arise with interferences that
102 cause inaccurate measurements when Gd is run as an oxide, so measurement as Gd^+ is preferred
103 [22]. Given that sample material and time can be limited in a nuclear forensic investigation, here
104 we developed a new method to measure Gd isotopes using MC-ICPMS. Whereas previous TIMS
105 studies measured Gd^+ with ~1000ng of Gd [*e.g.,* 20, 22], here we show that 100ng Gd can be
106 measured via MC-ICPMS and achieve similar precision. We applied this new method to a set of
107 25 UOCs previously investigated for their Sm and Nd isotope compositions [9, 16]. This Gd
108 isotope data is then used in conjunction with their Sm isotope compositions to place constraints

on the neutron energy spectra occurring in U ore bodies and to evaluate if Gd isotopes could be used as a new tool in nuclear forensics investigations.

2. Experimental

2.1. Samples investigated

This study investigated a diverse set of UOCs obtained from the sample library at Lawrence Livermore National Laboratory (LLNL), most of which have previously been analyzed for their Sm isotope compositions [16]. Table 1 provides a list of the samples along with their country of origin, sample mass, Gd concentrations, and deposit type. The UOC samples were previously processed to isolate and purify Sm, and details regarding the sample digestion and chemical procedures are provided in [16]. Briefly, samples were dissolved using 3 mL of 10.5 M HCl and 50 μL of concentrated HF. Next, Sm was isolated and purified from the UOC matrices using a three-step ion-exchange chromatography procedure. The final step of this procedure isolates Sm from other REEs using LN resin. The washes from this final column containing Gd were saved for all samples and used subsequently in the present study. Additionally, our sample set includes the certified UOC reference materials CUP-2 and UPER-1, the geostandards standards BCR-2 and BHVO-2, and a procedural blank.

Table 1 Sample information for the investigated UOCs and associated standards

Sample	Country	~mass (mg)	~Gd (μg/g)	Deposit type
Olympic Dam	Australia	1047	0.23	Hematite Breccia Complex
Radium Hill	Australia	30	40.7	Intrusive
Rum Jungle	Australia	86	3.4	Unconformity
Nuclebras	Brazil	145	2.6	Intrusive
Blind River	Canada	142	4.4	QP conglomerate
Denison	Canada	12	123	QP conglomerate
Dyno	Canada	137	4.5	Intrusive/Vein
Eldorado	Canada	55	24.9	Vein
Gunnar	Canada	47	8.9	Vein
Macassa	Canada	40	8.6	Intrusive
Madawaska	Canada	57	6.0	Intrusive
North Span	Canada	138	4.7	QP conglomerate
Rayrock	Canada	49	9.1	Vein
Rio Algom	Canada	17	60.0	QP conglomerate
Stanleigh	Canada	74	5.5	QP conglomerate
Stanrock	Canada	95	6.6	QP conglomerate
Brunhilde	Germany	84	6.1	Vein
Ellweiler	Germany	100	5.0	Rhyolite hosted
Wismut	Germany	71	2.8	Sandstone-Tabular/Vein/Lignite-coal
Feldioara	Romania	111	4.5	Sandstone-Tabular/Metamorphite
Nufcor	South Africa	100	8.7	QP conglomerate
Anaconda	USA	70	5.6	Sandstone-Tabular
Cotter	USA	129	5.7	Sandstone/Vein
Pathfinder	USA	84	4.5	Sandstone-Rollfront
Mindola	Zambia	52	303	Vein
UPER-1*	unknown	929	0.2	unknown
CUP-2*	Canada	1228[a]	0.6	QP conglomerate

*Denotes a certified UOC reference material

[a]An aliquot of this material was used to isolate and purify Sm and Gd

QP = quartz pebble

2.2. Chemical separation of Gd

All chemical reagents used in this study were Seastar™ high purity acids. All acids were diluted with 18.2 MΩ cm H_2O (Millipore Milli-Q®, hereafter "MQ") as needed. Given that the REEs have been separated from the UOC matrices in a previous study [16], the purification of

Gd required only one additional column before isotopic measurement. For this purpose, BioRad Glass Econo-Columns® filled with TrisKem LN Resin (100-150 μm) were used to separate and purify Gd from the other REEs (Table 2), modified from the procedure described in [23] but focusing just on the Gd purification. After resin cleaning and conditioning, the samples were loaded in 0.5 mL of 0.25M HCl. Then a 19 mL rinse of 0.25M HCl was added to the column followed by a 4 mL rinse of 0.4M HCl. Subsequently, a 6.5mL rinse of 0.55M HCl was added to the column followed by 1 mL of 0.75M HCl. Gadolinium was eluted using 8 mL of 0.75M HCl. The Gd cuts were evaporated to dryness and were processed through this procedure a second time to ensure isobaric interferences from Sm and Dy isotopes were sufficiently low before isotopic measurement. Typical yields of Gd from this procedure are > 90%. The certified reference materials UPER-1 and CUP-2 were processed through the full analytical procedure described in [16] to separate Sm and subsequently processed through the procedure described here to purify Gd analogously to the UOCs. The total procedural blank was 115pg Gd, which is negligible considering that all samples investigated here had ~200ng Gd or more. All samples were dried to completion and treated with 0.5mL concentrated HNO_3 before dissolution in 2% HNO_3 for isotopic measurement.

153 **Table 2** The chemical separation procedure used to purify Gd from other REEs

Eluent	Volume	Description
LN Resin 100-150 μm (in Glass Econo-columns®)		
~6M HCl	5	clean
MQ H_2O	1	clean
~6M HCl	5	clean
MQ H_2O	1	clean
0.25M HCl	5	condition
0.25M HCl	0.5	load
0.25M HCl	19	rinse
0.4M HCl	4	rinse
0.55M HCl	6.5	rinse
0.75M HCl	1	rinse
0.75M HCl	8	**Gd**

154
155

156 *2.3. Mass spectrometry*

157 All Gd isotope ratio measurements were carried out on a Thermo Scientific® Neoma MC-
158 ICPMS at LLNL. Samples were introduced as 100 ng/g Gd solutions using an Apex Omega as
159 well as Jet sample and H skimmer cones. A single line routine was used to collect all isotopes of
160 Gd along with ^{149}Sm, ^{150}Sm, and ^{161}Dy using Faraday cups connected to 10^{11} Ω resistors. Using
161 this set-up, the typical sensitivity on ^{158}Gd was ~7.5 volts. Samples and standards were measured
162 for 100 cycles of 4 s integration times each and samples were measured at least three times when
163 possible. Samples were bracketed with a Gd standard solution from Inorganic Ventures. Data
164 were corrected for instrumental mass fractionation using the exponential law and by internally
165 normalizing to (^{155}Gd + ^{156}Gd)/^{160}Gd = 1.61294 [22]. This three-isotope normalization scheme
166 was selected to consider any isotopic shift from the neutron capture on ^{155}Gd (which transmutes
167 to ^{156}Gd) that occurs in neutron-irradiated samples. The Gd isotope data are reported utilizing the
168 ε-notation, or parts per ten thousand deviations from the bracketing solution standard using (1).

$$\varepsilon^{i}Gd_{sample} = \left(\frac{\left({}^{i}Gd/{}^{160}Gd \right)_{sample}}{\left({}^{i}Gd/{}^{160}Gd \right)_{standard}} - 1 \right) \times 10{,}000 \quad (1)$$

In (1), *i* represents the isotope of interest (*e.g.*, ^{157}Gd or ^{158}Gd). For CUP-2 and UPER-1, their Sm isotopic compositions were measured via MC-ICPMS at LLNL using the same instrument set-up as was done for Gd with the exception that data was collected in 30 cycles of 8 s integration times. Data were corrected for instrumental mass fractionation using the exponential law and by internally normalizing to ^{147}Sm/^{152}Sm = 0.56081. The Sm isotopic results are reported in Table 3 along with the Gd isotopic results.

3. Results

3.1 Accuracy of Gd isotope measurements

Only one prior study was found to have measured Gd isotopes using MC-ICPMS [24] and because Gd isotope measurements are not commonplace via MC-ICPMS, we performed doping tests to quantify the levels of isobaric interferences that are tolerable without affecting the isotope measurements. Whereas two isotopes of Sm (*i.e.,* ^{152}Sm, ^{154}Sm) interfere directly on isotopes of Gd (*i.e.,* ^{152}Gd, ^{154}Gd), these low abundance Gd isotopes are not the focus of this study as they are not relevant for neutron capture reactions. As such, the Gd isotopes of interest in this work (*i.e.,* ^{155}Gd, ^{156}Gd, ^{157}Gd, ^{158}Gd, ^{160}Gd) only have isobaric interferences from Dy isotopes. Therefore, these doping tests were limited to solutions doped with variable concentrations of Dy. The results from these tests are presented in Fig. 1 and demonstrate that our upper threshold for isobaric interferences from Dy isotopes are around Gd/Dy = 5000. All unknown samples measured in this work had Gd/Dy<5000. Additionally, the results of the geostandards BCR-2 and BHVO-2 are presented in Table 3. Both geostandards have

indistinguishable Gd isotope compositions compared to the bracketing Gd standard, demonstrating the accuracy of the method employed here. Given that BCR-2 and BHVO-2 are both basalts, and consequently they do not have a significant amount of U to generate neutrons, one should not expect to see neutron capture effects in these two geostandards. The external reproducibility of the method determined by multiple analyses of the geostandards BCR-2 and BHVO-2 was ±0.11 for ε^{157}Gd and ±0.09 for ε^{158}Gd (Table 3). Uncertainties represent either the 2 × standard deviation (2SD) of multiple measurements or the external reproducibility of the method, whichever was larger.

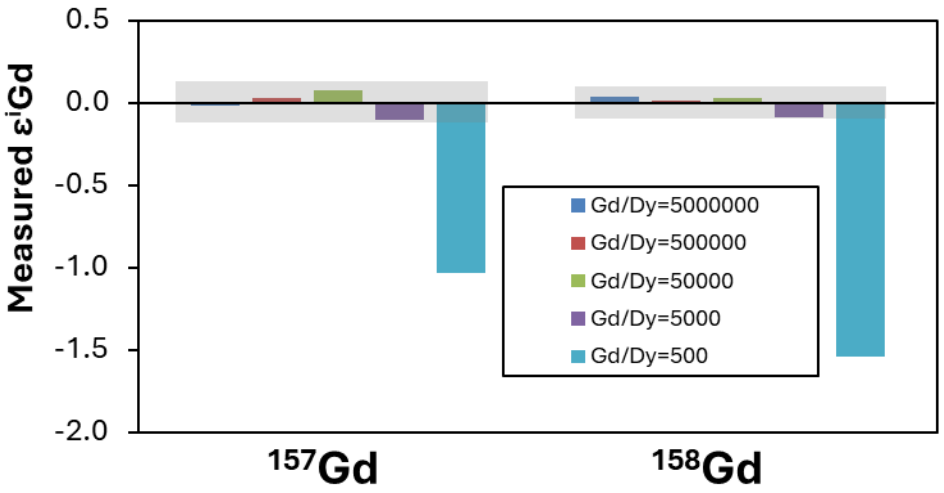

Fig. 1 Shown are the ε^{157}Gd and ε^{158}Gd isotopic differences for 100 ng/g solutions doped with varying amounts of Dy. The light grey box is the external reproducibility of our method. Measured isotope ratios are accurate as long as Gd/Dy is ≥5,000

3.2 Gd isotope compositions of UOCs

The Gd isotope compositions of the UOC samples are presented in Table 3 and Fig. 2. Approximately half of the UOCs exhibit ε^{157}Gd and ε^{158}Gd values that are indistinguishable within analytical uncertainty from the solution standard, whereas the remaining half display ε^{157}Gd and ε^{158}Gd values that are resolved from the solution standard.

Table 3 The Gd and Sm isotope compositions of the UOCs and standards. The Gd isotope ratios are backcalculated using the epsilon anomalies and natural Gd isotope compositions of 0.71592 and 1.136322 for $^{157}Gd/^{160}Gd$ and $^{158}Gd/^{160}Gd$, respectively. Mass bias is corrected using the exponential law and internally normalizing to $(^{155}Gd + ^{156}Gd)/^{160}Gd = 1.61294$ [22]

Sample	*n*	$^{157}Gd/^{160}Gd$	unc	$^{158}Gd/^{160}Gd$	unc	$\varepsilon^{157}Gd$	unc	$\varepsilon^{158}Gd$	unc	*n*	$\varepsilon^{149}Sm^*$	$\varepsilon^{150}Sm^*$
Anaconda	3	0.715918	0.000008	1.136328	0.000010	-0.02	0.11	0.06	0.09		0.03	0.25
Blind River	3	0.715894	0.000008	1.136346	0.000010	-0.36	0.11	0.21	0.09		-0.14	0.71
Cotter	3	0.715911	0.000008	1.136338	0.000010	-0.12	0.11	0.14	0.09		-0.02	0.28
Dyno	2	0.715866	0.000008	1.136382	0.000010	-0.75	0.11	0.53	0.09		-0.36	0.72
Gunnar	3	0.715866	0.000008	1.136374	0.000010	-0.74	0.11	0.45	0.09		-0.31	0.86
Macassa	5	0.715918	0.000008	1.136323	0.000010	-0.02	0.11	0.01	0.09		0.00	0.07
North Span	3	0.715896	0.000010	1.136348	0.000010	-0.33	0.14	0.22	0.09		-0.21	0.36
Nufcor	3	0.715902	0.000008	1.136342	0.000010	-0.25	0.11	0.18	0.09		-0.06	0.43
Radium Hill	3	0.715917	0.000008	1.136334	0.000015	-0.04	0.11	0.11	0.13		-0.03	0.12
Rayrock	3	0.715852	0.000009	1.136388	0.000010	-0.95	0.12	0.58	0.09		-0.44	1.06
Rio Algom	3	0.715899	0.000008	1.136345	0.000010	-0.29	0.11	0.21	0.09		-0.17	0.55
Olympic Dam	1	0.715904	0.000008	1.136344	0.000010	-0.21	0.11	0.20	0.09		-0.11	0.32
Nuclebras	2	0.715917	0.000008	1.136320	0.000010	-0.03	0.11	-0.02	0.09		0.03	-0.05
Denison	15	0.715895	0.000008	1.136347	0.000010	-0.34	0.11	0.22	0.09		-0.17	0.56
Mindola	10	0.715905	0.000008	1.136344	0.000010	-0.20	0.11	0.20	0.09		-0.15	0.44
Eldorado	5	0.715886	0.000008	1.136361	0.000012	-0.47	0.11	0.34	0.11		-0.27	0.83
Brunhilde	2	0.715879	0.000008	1.136378	0.000010	-0.57	0.11	0.49	0.09		-0.29	0.68
Eilweiler	3	0.715881	0.000008	1.136368	0.000010	-0.54	0.11	0.40	0.09		-0.25	0.66
Feldiora	3	0.715922	0.000008	1.136327	0.000010	0.03	0.11	0.04	0.09		-0.02	0.08
Pathfinder	3	0.715925	0.000008	1.136322	0.000010	0.08	0.11	0.00	0.09		-0.01	-0.06
Rum Jungle	3	0.715870	0.000008	1.136376	0.000010	-0.69	0.11	0.47	0.09		-0.26	0.83
Stanleigh	3	0.715889	0.000008	1.136349	0.000010	-0.43	0.11	0.24	0.09		-0.29	0.58
Stanrock	3	0.715907	0.000008	1.136340	0.000010	-0.17	0.11	0.16	0.09		-0.11	0.34
Wismut	1	0.715920	0.000008	1.136333	0.000010	0.01	0.11	0.10	0.09		0.04	0.10
Madawaska	3	0.715912	0.000008	1.136319	0.000010	-0.10	0.11	-0.02	0.09		-0.05	0.08
UPER-1	2	0.715920	0.000008	1.136327	0.000010	0.01	0.11	0.04	0.09	2	0.02	-0.08
CUP-2	3	0.715908	0.000008	1.136342	0.000011	-0.16	0.11	0.17	0.10	6	-0.26	0.37
BCR-2	7	0.715923	0.000009	1.136323	0.000010	0.05	0.12	0.01	0.09			
BHVO-2	7	0.715919	0.000008	1.136325	0.000010	0.00	0.11	0.02	0.09			
Geostandards[a]	14	0.715921	0.000008	1.136324	0.000010	0.02	0.11	0.02	0.09			

*$\varepsilon^{149}Sm$ and $\varepsilon^{150}Sm$ data are from [16], except for UPER-1 and CUP-2, which were analyzed in this study.

[a]Geostandards represent the average of BCR-2 and BHVO-2.

Uncertainties (±) represent either the 2 × standard deviation (2SD) of multiple measurements or the external reproducibility of the method, whichever was larger, and are given as the last digits in the value. Uncertainties (2SD) on $\varepsilon^{149}Sm$ and $\varepsilon^{150}Sm$ measured in this work are 0.16 and 0.18, respectively.

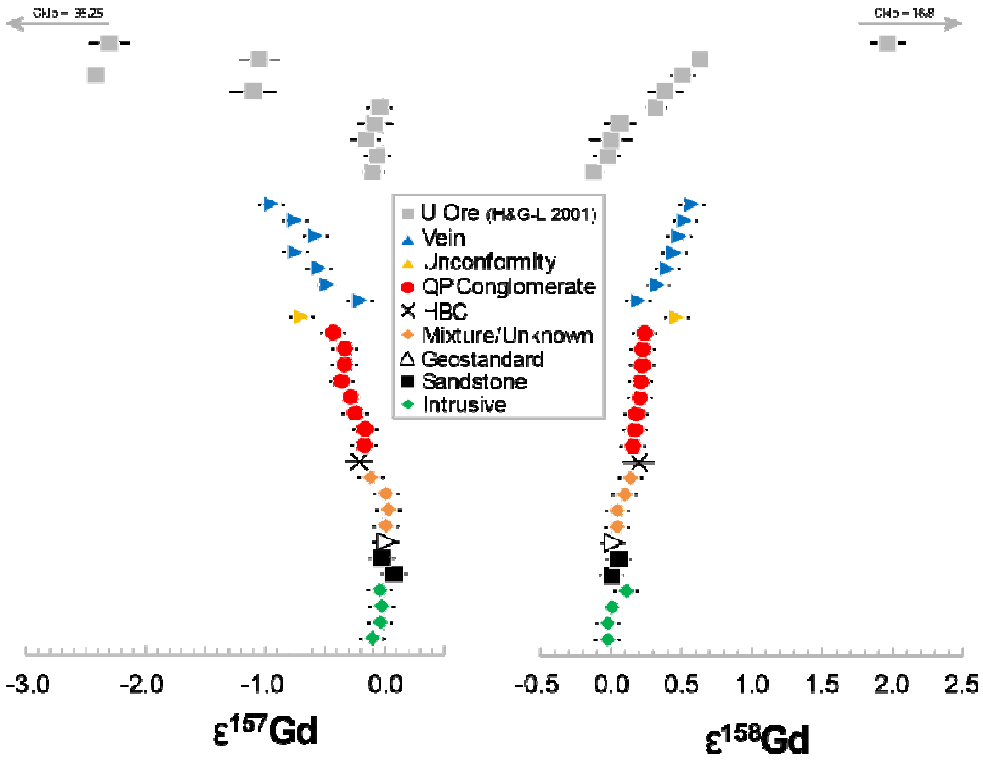

Fig. 2 The ε^{157}Gd and ε^{158}Gd isotope compositions of the UOCs (color) and literature data (gray) for U ores. The deviation of all samples relative to the solution standard is given in ε-notation. Individual sample uncertainties represent 2SD. U ore data from [19], with the note that the values for the Oklo deposit are far off-scale. "Geostandard" is the average of BCR-2 and BHVO-2 measured in this work, as shown in Table 1

3.3 Sm isotope compositions of UOC reference materials

The Sm isotope compositions of the UOC reference materials CUP-2 and UPER-1 are presented in Table 3. CUP-2 exhibits a depletion in ε^{149}Sm of -0.26 ± 0.16 (2SD) coupled with an excess in ε^{150}Sm of 0.37 ± 0.18 (2SD). These results are consistent within the analytical uncertainties of CUP-2 Sm isotopic data from [16] that reported ε^{149}Sm of -0.32 ± 0.19 and ε^{150}Sm of 0.66 ± 0.21. UPER-1, which was not measured in [16], displays ε^{149}Sm and ε^{150}Sm values that are indistinguishable from the solution standard.

4. Discussion

234 *4.1. Consideration of nuclear field shift in Gd isotopes*

235 Deviations from the natural Gd isotopic composition are evident in many of the UOC samples
236 studied here. High-precision isotope ratio measurements of other REEs like Sm, Nd, Er, and Yb
237 have demonstrated that isotopic shifts can be induced by chemical purification using LN resin
238 and DGA resin, especially when chemical yields are low [25-27]. These isotopic shifts have been
239 attributed to the nuclear field shift effect which is a natural mass-independent isotope
240 fractionation caused by differences in the size, shape, and charge between nuclei during chemical
241 exchange reactions [*e.g.,* 28-29]. Therefore, before interpretation of the Gd isotope data of the
242 UOCs, it is important to exclude that the ε^{157}Gd and ε^{158}Gd values are not impacted by the
243 nuclear field shift effect. As the yields of our chemical processing are >90% and both
244 geostandards BCR-2 and BHVO-2 have Gd isotope compositions indistinguishable from the Gd
245 solution standard, this suggests that the nuclear field shift is not a concern in the present work.
246 Furthermore, and as is discussed in the next section, the UOCs fall on the theoretical trend for
247 thermal neutron capture effects.

248

249 *4.2. Thermal neutron capture effects in UOCs*

250 Comparing the ε-values visually in Fig. 2, it is evident that these negative anomalies in ε^{157}Gd
251 and positive anomalies in ε^{158}Gd are related to one another. Furthermore, also shown in Fig. 2
252 are U ores previously measured in [19]. In ε^{158}Gd, the UOCs span a range from ~ 0 to 0.5
253 whereas the U ores span a slightly larger range from ~ 0 to 2, except for one ore from the Oklo
254 natural reactor that has an ε^{158}Gd of ~19. The observation that U ores have a larger range of Gd
255 isotope compositions (Fig. 2) compared to UOCs can be readily explained by the fact that UOCs
256 are typically produced from several different U ores and potentially different mines in a similar

257 geographic location and, thus, represent average isotopic compositions of their parental U ore
258 material.

259 Due to the difficulty in directly determining absolute isotopic ratios using an MC-ICPMS
260 during a measurement campaign, the ε-values displayed in Fig. 2 were determined relative to a
261 solution standard that bracketed the unknowns. However, absolute Gd isotopic ratios for the
262 samples were backcalculated from the determined ε-values of the samples using the assumed
263 natural compositions of $^{157}Gd/^{160}Gd=0.71592$ and $^{158}Gd/^{160}Gd=1.136322$ and are displayed in
264 Fig. 3. From Fig. 3, it is clear that $^{157}Gd/^{160}Gd$ and $^{158}Gd/^{160}Gd$ are highly anticorrelated and
265 follow the predicted behavior of the 1:1 transmutation into ^{158}Gd when a ^{157}Gd atom captures a
266 thermalized neutron (dashed line slope = -1, Fig. 3). Similar to prior work on the Sm isotopic
267 system [16], the observed Gd isotope variations are readily explained by neutron capture
268 processes in the Gd isotopes.
269

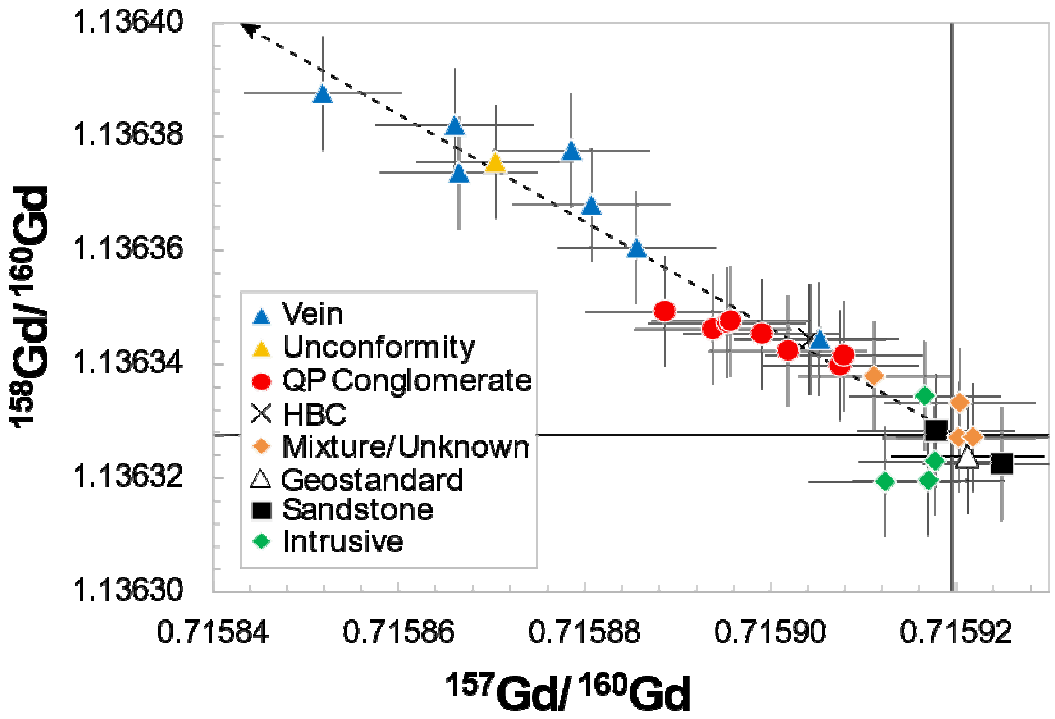

Fig. 3 The $^{158}Gd/^{160}Gd$ vs. $^{157}Gd/^{160}Gd$ of the UOCs and geostandard from this work. Individual sample uncertainties are 2SD. The dashed line is the predicted behavior (slope = -1) when ^{157}Gd captures a neutron, transmuting to ^{158}Gd. Geostandard is the average of BCR-2 and BHVO-2 measured in this work

As previously detailed, the effects of neutron capture reactions are preserved in the Gd isotopic system in samples derived from the beginning stages of the nuclear fuel cycle. While prior work had shown these effects to be present in U ore samples [19], extending this capability to UOC is helpful for nuclear forensics, as UOC is an attractive material for smugglers [1]. While it is possible that background Gd could be present during U ore processing and UOC production, the fact that the UOCs still plot along a -1 slope in Fig. 3 demonstrates that they retain neutron capture signatures from their parental ores following processing. This demonstrates the robustness of the REE isotopic signatures of UOCs, as shown now in Gd (this work), Sm [16], and Nd [8-9].

4.3. Origin assessment of UOCs

For measurable isotopic perturbations caused by neutron capture reactions to occur in an ore deposit, certain conditions are logically required. First, there must be a source of neutrons: in the case of a U ore deposit, the most likely source of neutrons is either spontaneous or induced fission of uranium. As such, deposits with higher grades (*i.e.,* content) of uranium would have a higher likelihood of capturing neutrons compared to deposits with lower grades of uranium. Secondly, there must be ample time for measurable isotopic perturbations to develop, so ancient ore deposits (~> 1.5Ga) are more likely to have measurable isotopic shifts than younger deposits, particularly because the abundance of ^{235}U (currently 0.7%) was higher (~3%) earlier in Earth's history. Lastly, because the probability of neutron capture increases for Sm and Gd when a neutron is "thermalized", or loses much of its kinetic energy, ore deposits moderated by a water table (*i.e.,* Oklo natural reactor) will theoretically produce larger neutron capture signatures in Sm and Gd than unmoderated deposits with similar characteristics. All of these conditions play a role in the neutron capture processes for Gd and Sm—to various extents at various times in the deposit history—and it can be difficult to untangle. This difficulty is illustrated in Fig. 4 with plots of $\varepsilon^{158}Gd$ versus age of the deposit and $\varepsilon^{158}Gd$ versus U ore grade, which lack clear correlations in the data.

Similar to what was recognized within the Sm isotopic system [16], UOCs sourced from vein, unconformity, and QP conglomerate deposits appear more likely to display shifts in $^{158}Gd/^{160}Gd$ and $^{157}Gd/^{160}Gd$ than samples from other types of ore deposits (Fig. 3). Although these shifts are due to a combination of ore body age, grade, and composition, for many samples, it appears that longevity of exposure to thermalized neutrons is important (Fig. 4). For example, all UOCs older

than 1.5Ga have resolved positive shifts in ε^{158}Gd whereas few samples younger than 1.5Ga show any deviation from the standard values. Whereas some UOCs with higher ore grades have resolved ε^{158}Gd, not all do, perhaps because the range in uranium grade is not as extreme as the range in ages for uranium ore deposits. This could also be due to circumstances associated with neutron moderation that are not captured in the rock record. Either way, for this sample set, all UOCs with ore material that is older than 1.5Ga are anomalous in ε^{158}Gd and, therefore, it appears that the age of the ore deposit is a major factor driving if measurable neutron capture effects are present or not in a UOC sample. Importantly, if an interdicted UOC has isotopic shifts in ε^{157}Gd and ε^{158}Gd, this suggests that its parental U ore was likely older than 1.5Ga. In contrast, an interdicted UOC without isotopic shifts in ε^{157}Gd and ε^{158}Gd would suggest it originated from a younger ore body, although we cannot fully exclude that the Gd isotope composition is affected by natural Gd added during the UOC production process. Future work comparing Gd isotope compositions of paired U ore with UOC would help better understand the amount of natural Gd added during processing.

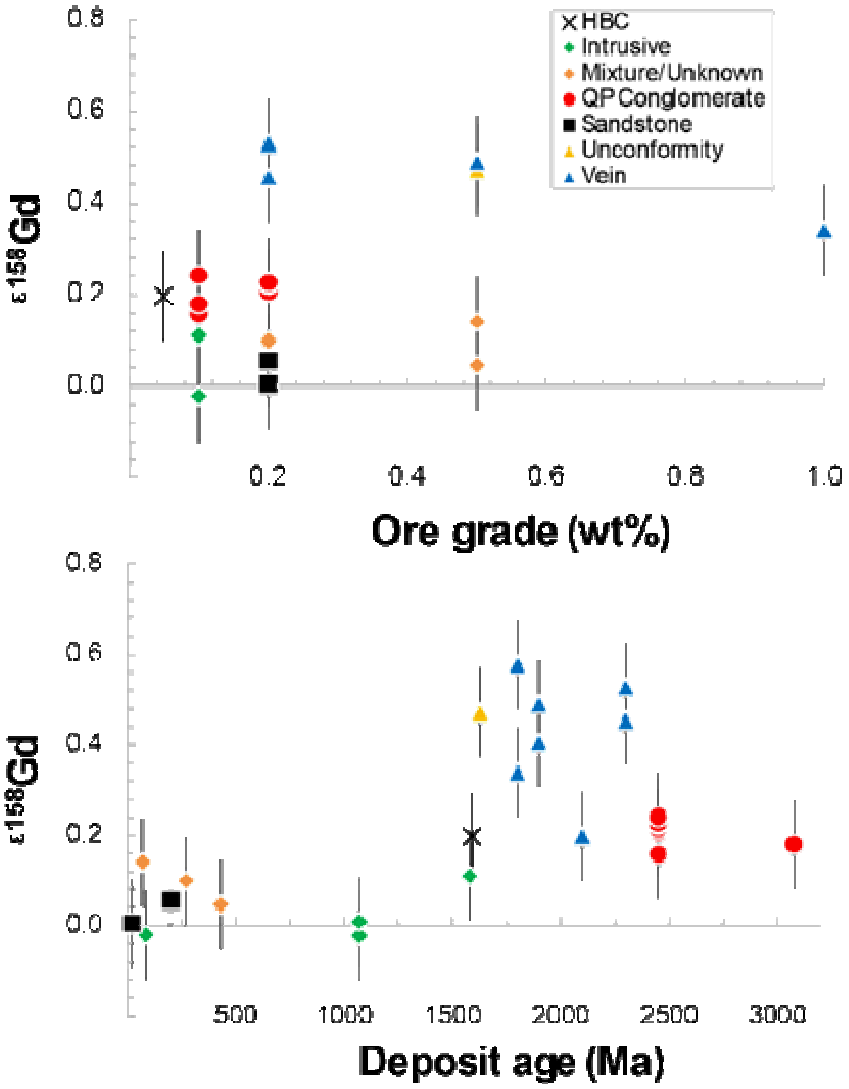

325

326 **Fig. 4** The ε^{158}Gd vs. ore grade (wt%) (top panel) and vs. deposit age (bottom panel). Individual
327 sample uncertainties for the y-axis are 2SD. Age and grade of deposits taken from [16]
328

4.4. Neutron fluence and neutron energy spectrum as a new nuclear forensic signature of UOCs

The Gd isotope compositions of the UOCs measured here and the Sm isotope compositions previously measured on the same samples can be used to determine information about the neutrons that caused these isotope variations. Shown in Fig. 5 is a plot of the ε^{158}Gd versus ε^{150}Sm for the UOCs. Overall, the ε^{158}Gd and ε^{150}Sm values of the UOCs are well-correlated. This type of linear correlation has been observed previously in other natural samples including certain meteorites and samples from the Moon [21, 30-31]. The linear correlation between Sm and Gd isotopes is due to thermalized neutrons within the specific ore bodies.

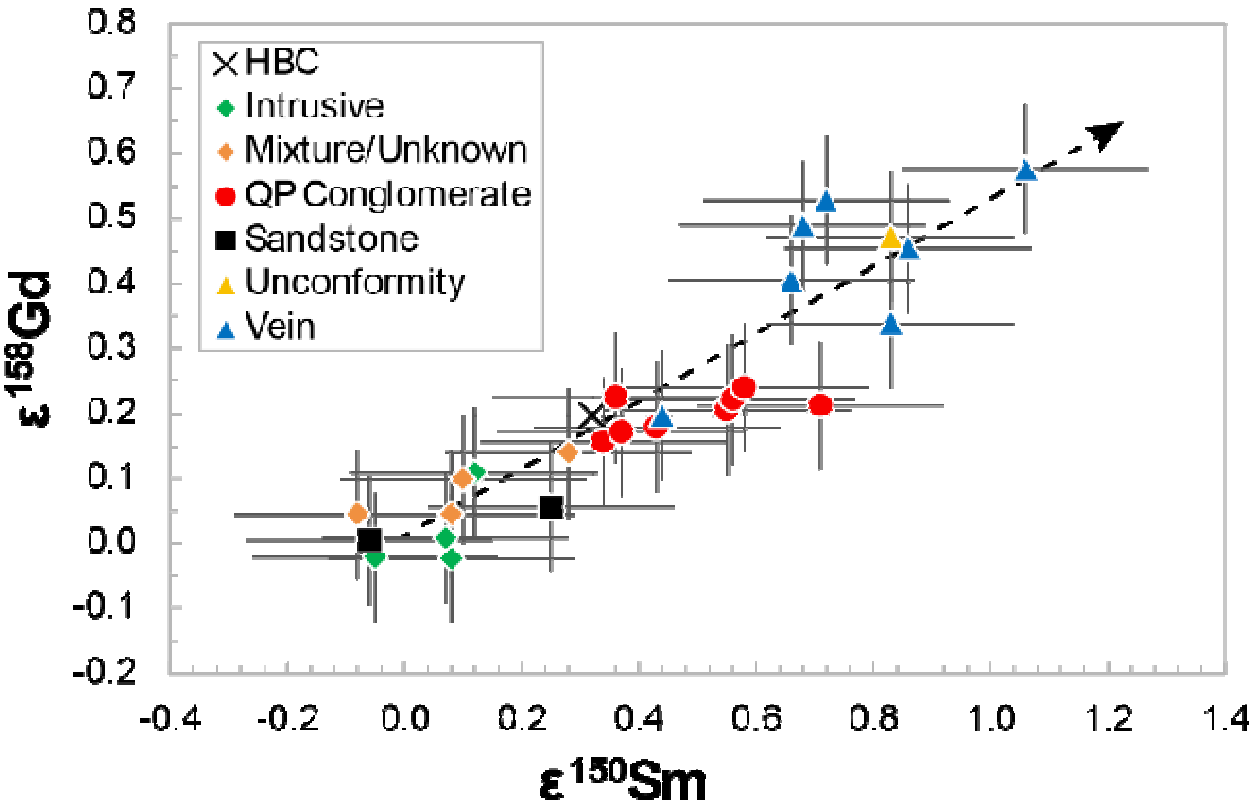

Fig. 5 The ε^{150}Sm vs. ε^{158}Gd for the UOCs of this study. Individual sample uncertainties are 2SD. The dotted line is the correlation line for the UOCs set at the origin

Information about the neutron fluence and the neutron energy spectrum could complement other material signatures utilized in a nuclear forensics investigation and provide direct information on the parental U ore body. Specifically, the neutron capture effects in the UOCs can be used to calculate the neutron fluence they experienced. Previous studies investigating U ore samples have calculated the neutron fluence based on either $^{150}Sm/^{149}Sm$ or $^{158}Gd/^{157}Gd$ [19, 32]. For UOCs that had resolved $\varepsilon^{150}Sm$ isotope compositions, we performed a similar calculation to estimate the neutron fluence following the methods of [21] and using (2).

$$\Psi = \frac{\left(^{150}Sm/^{149}Sm\right)_{sample} - \left(^{150}Sm/^{149}Sm\right)_{Std}}{\left(^{150}Sm/^{149}Sm\right)_{STD2} - \left(^{150}Sm/^{149}Sm\right)_{Std}} \times \frac{(\sigma)_{STD2}}{(\sigma)_{sample}} \times (5.94 \times 10^{15}) \qquad (2)$$

In (2), $^{150}Sm/^{149}Sm_{sample}$ was calculated here (Table 4) using the Sm isotope data from [16], STD2 is an irradiated standard that has a known neutron fluence of 5.94×10^{15} n/cm^2 [19], Std is the non-irradiated standard [19], and σ is the ^{149}Sm thermal neutron capture cross section. Note that the value employed here for $(^{150}Sm/^{149}Sm)_{Std}$ is 0.533974 as determined from multiple analyses of BCR-2 and BHVO-2, compared to the value of 0.533995 of the non-irradiated Std from [19]. To account for this offset, we adjusted the STD2 and Std values reported in [19] by the offset 0.000021 and then calculated the neutron fluence of the UOCs (Table 4). We selected the Sm isotopic system to calculate neutron fluence as these UOCs were measured with TIMS like in [19]. Overall, the UOCs have neutron fluences on the order of 10^{14} n/cm^2. This range in neutron fluence is similar to results from four U ores (Fig. 6; [19]), however, this range is smaller in magnitude compared to the five Olympic Dam ores with neutron fluences around 10^{15} n/cm^2 [32]. In comparison, the Oklo natural reactor has neutron fluences around 10^{21} n/cm^2 [33-35]

while the Moon and certain meteorites have neutron fluences on the order of 10^{16} n/cm^2 [21, 30-31]. Therefore, the neutron fluences recorded by the UOCs are at the lower end compared to other measured natural materials (Fig. 6). Given that UOCs are often produced from numerous U ores from a regional geographic area with variable compositions, the smaller range in neutron fluence for the UOCs reflects the averaging of the parent U ore material. For example, [32] measured 40 ores from the Olympic Dam deposit and only five had measurable neutron capture effects in the Sm isotopic system. Therefore, it is unsurprising that the Olympic Dam UOC reported here has an "average" neutron fluence on the order of ~2 $\times 10^{14}$ n/cm^2 while certain individual ores were about an order of magnitude higher [32].

Table 4 The $^{150}Sm/^{149}Sm$, $^{158}Gd/^{157}Gd$, neutron fluence (ψ), and $\varepsilon_{Sm}/\varepsilon_{Gd}$ of the UOCs. These calculations were only performed on samples that had resolved $\varepsilon^{150}Sm$ anomalies

Sample	$^{150}Sm/^{149}Sm$	±	$^{158}Gd/^{157}Gd$	±	ψ	εSm/εGd	±
Denison	0.534017	13	1.587309	23	6.11E+14	0.81	0.45
Eldorado	0.534037	13	1.587349	24	9.07E+14	0.82	0.32
Olympic Dam	0.534002	13	1.587285	23	4.00E+14	0.72	0.59
Gunnar	0.534041	13	1.587410	23	9.64E+14	0.59	0.19
Blind River	0.534022	13	1.587311	23	6.92E+14	0.88	0.46
Mindola	0.534010	13	1.587283	23	5.13E+14	0.95	0.68
Rayrock	0.534058	13	1.587462	24	1.21E+15	0.58	0.15
Stanrock	0.534002	13	1.587272	23	4.00E+14	0.89	0.80
Dyno	0.534037	13	1.587423	23	8.98E+14	0.52	0.17
Stanleigh	0.534025	13	1.587327	23	7.28E+14	0.80	0.37
Brunhilde	0.534029	13	1.587389	23	7.83E+14	0.55	0.21
Rio Algom	0.534017	13	1.587298	23	6.11E+14	0.92	0.54
Rum Jungle	0.534035	13	1.587404	23	8.79E+14	0.56	0.19
Ellweiler	0.534027	13	1.587371	23	7.53E+14	0.59	0.24
North Span	0.534009	13	1.587309	26	5.02E+14	0.66	0.43
Nufcor	0.534005	13	1.587288	23	4.39E+14	0.76	0.57
CUP-2	0.534008	13	1.587273	23	4.87E+14	1.06	0.86
Terrestrial Avg.	0.533974	13	1.587219	23			

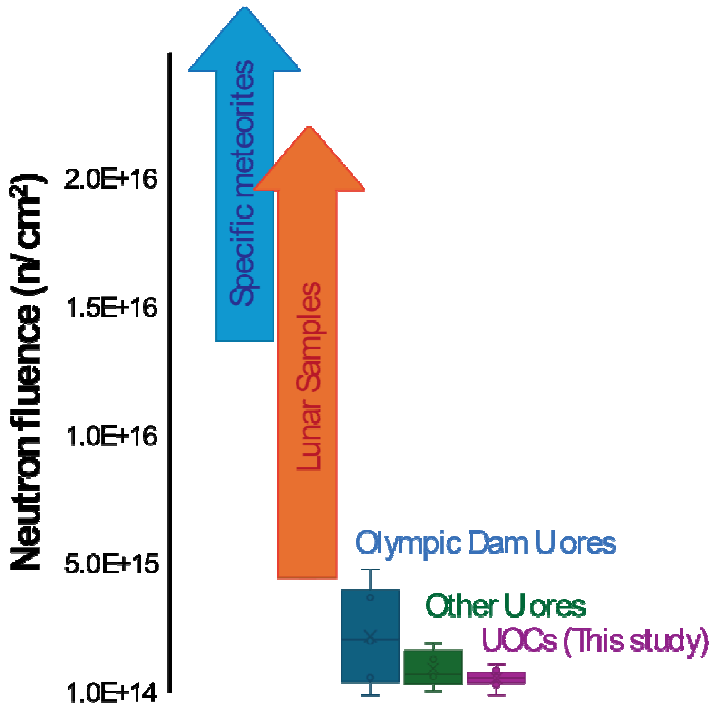

Fig. 6 Plot of neutron fluence ranges in n/cm^2 for the UOCs of this work along with U ores, meteorites, and lunar samples [19, 21, 30-32]. Meteorites and the Moon go off this plot to ~10^{17} n/cm^2

As both Sm and Gd isotope compositions were measured on the UOCs, the neutron energy spectrum defined as $\varepsilon_{Sm}/\varepsilon_{Gd}$ can be calculated. The neutron energy spectrum provides information regarding the energy of the neutrons that were captured by both ^{149}Sm and ^{157}Gd. This calculation was done using (3) and following the method of [21].

$$\frac{\varepsilon Sm}{\varepsilon Gd} = \frac{\frac{\left(^{150}Sm/^{149}Sm\right)_{sample} - \left(^{150}Sm/^{149}Sm\right)_{Std}}{1+\left(^{150}Sm/^{149}Sm\right)_{sample}}}{\frac{\left(^{158}Gd/^{157}Gd\right)_{sample} - \left(^{158}Gd/^{157}Gd\right)_{Std}}{1+\left(^{158}Gd/^{157}Gd\right)_{sample}}} \quad (3)$$

In (3), $^{150}Sm/^{149}Sm_{sample}$ and $^{158}Gd/^{157}Gd_{sample}$ are from Table 4 and $^{150}Sm/^{149}Sm_{Std}$ and $^{158}Gd/^{157}Gd_{Std}$ are from the geostandards BCR-2 and BHVO-2 measured in this work (Table 4). Differences in $\varepsilon_{Sm}/\varepsilon_{Gd}$ are controlled by the chemical composition and temperature of the target material [36] and because ^{149}Sm has a higher neutron capture resonance (0.0973 eV) compared to ^{157}Gd (0.0314 eV), a higher $\varepsilon_{Sm}/\varepsilon_{Gd}$ reflects that more energized neutrons were captured whereas a lower $\varepsilon_{Sm}/\varepsilon_{Gd}$ reflects that more thermalized neutrons were captured [21]. The $\varepsilon_{Sm}/\varepsilon_{Gd}$ of the UOCs are shown in Table 4 and have a range in $\varepsilon_{Sm}/\varepsilon_{Gd}$ of 0.52 to 1.05. For comparison, five U ores from [19] had a range in $\varepsilon_{Sm}/\varepsilon_{Gd}$ of 0.003 to 0.81, similar to the UOCs, while meteorite samples with neutron fluences around 10^{16} n/cm^2 had a range in $\varepsilon_{Sm}/\varepsilon_{Gd}$ of 1.38 to 15.01 [21]. While the calculated numbers are perhaps not initially intuitive, the fact that extraterrestrial samples experienced significantly higher neutron energies compared to terrestrial ore deposits makes sense due to the lack of moderators (*e.g.,* water) on extraterrestrial bodies.

The combined Sm and Gd isotope compositions of the UOCs provide a new tool that can be utilized in nuclear forensics. For an unknown UOC with measurable shifts in the neutron capture isotopes of Sm and Gd, information regarding the neutron fluence and neutron energies can be extracted and also provides information on the type and general age of the parental U ore deposit. Additionally, samples without neutron capture effects in Sm and Gd also suggest specific types of parental deposits where samples could have originated. Such information will be best utilized in conjunction with other material signatures and comparison to known UOC samples.

5. Conclusions

This work presents a new method for the isotope measurement of Gd with applications to geology, cosmochemistry and nuclear forensics using MC-ICPMS. This novel method allows for the measurement of small amounts of sample (~100ng Gd) and quicker throughput (~1 day) compared to TIMS analyses that typically require 1000ng and can take several days. This method was applied to a set of UOCs, revealing that approximately half the samples contain isotopically anomalous Gd caused by thermal neutron capture processes in the parental U ore bodies. In general, UOCs derived from older deposits with higher U contents have resolved Gd isotope compositions whereas UOCs derived from younger deposits with less U contents do not show evidence of thermal neutron capture. The thermal neutron capture effects in Gd isotopes are correlated with Sm neutron captures isotopes measured on the same UOCs. The combined Gd and Sm neutron capture data is used to estimate the neutron fluence and neutron energy spectrum of the samples, demonstrating a novel tool for nuclear forensics investigations.

Acknowledgements

This work was performed under the auspices of the U.S. Department of Energy by Lawrence Livermore National Laboratory under contract DE-AC52-07NA27344 with release number LLNL-JRNL-2003812.

Declarations

The authors have no relevant financial or non-financial interests to disclose.

References

[1] Kristo MJ, Gaffney AM, Marks N, Knight K, Cassata WS, Hutcheon ID (2016) Nuclear forensic science: analysis of nuclear material out of regulatory control, Annu. Rev. Earth Planet Sci. DOI 10.1146/annurev-earth-060115-012309

[2] Varga Z, Wallenius M, Krachler M, Rauff-Nisthar N, Fongaro L, Knott A, Nicholl A, Mayer K (2022) Trends and perspectives in Nuclear Forensic Science, Trends Anal. Chem. DOI 10.1016/j.trac.2021.116503

[3] Kristo MJ, Tumey SJ (2013) The state of nuclear forensics, Nucl. Instrum. Meth. B DOI 10.1016/j.nimb.2012.07.047

[4] Brennecka GA, Borg LE, Hutcheon ID, Sharp MA, Anbar A (2010) Natural variations in uranium isotope ratios of uranium ore concentrates: Understanding the $^{238}U/^{235}U$ fractionation mechanism, Earth Planet. Sci. Lett. DOI 10.1016/j.epsl.2010.01.023

[5] Spano TL, Simonetti A, Balboni E, Dorais C, Burns PC (2017) Trace element and U isotope analysis of uraninite and ore concentrate: applications for nuclear forensic investigations, Appl. Geochem. DOI 10.1016/j.apgeochem.2017.07.003

[6] Z. Varga Z, Wallenius M, Mayer K, Keegan E, Millet S (2009) Application of lead and strontium isotope ratio measurements for the origin assessment of uranium ore concentrates, Anal. Chem. DOI 10.1021/ac901100e

[7] Varga Z, Krajkó J, Peńkin M, Novák M, Eke Z, Wallenius M, Mayer K (2017) Identification of uranium signatures relevant for nuclear safeguards and forensics, J. Radioanal. Nucl. Chem. DOI 10.1007/s10967-017-5247-5

[8] Krajkó J, Varga Z, Yalcintas E, Wallenius M, Mayer K (2014) Application of neodymium isotope ratio measurements for the origin assessment of uranium ore concentrates, Talanta DOI 10.1016/j.talanta.2014.06.022

[9] Devlin McLoughlin VE, Shollenberger QR, Brennecka GA (2023) Determining provenance of uranium ore concentrates using 143Nd/144Nd, Talanta DOI 10.1016/j.talanta.2022.124088

[10] Švedkauskaitė-LeGore J, Rasmussen G, Abousahl S, van Belle P (2008) Investigation of the sample characteristics needed for the determination of the origin of uranium-bearing materials, J. Radioanal. Nucl. Chem. DOI 10.1007/s10967-007-7215-y

[11] Mercadier J, Cuney M, Lach P, Boiron MC, Bonhoure J, Richard A, Leisen M, Kister P (2011) Origin of uranium deposits revealed by their rare earth element signature, Terra Nova DOI 10.1111/j.1365-3121.2011.01008.x

[12] Keegan E, Wallenius M, Mayer K, Varga Z (2012) Rasmussen G, Attribution of uranium ore concentrates using elemental and anionic data, Appl. Geochem. DOI 10.1016/j.apgeochem.2012.05.009

[13] Varga Z, Wallenius M, Mayer K (2010) Origin assessment of uranium ore concentrates based on their rare-earth elemental impurity pattern, Radiochim. Acta DOI 10.1524/ract.2010.1777

[14] Rolison JM, Druce M, Shollenberger QR, Kayzar-Boggs TM, Lindvall RE, Wimpenny J (2019) Molybdenum isotope compositions of uranium ore concentrates by double spike MC-ICP-MS, Appl Geochem DOI 10.1016/j.apgeochem.2019.03.001

[15] Sullivan DL, Brennecka GA, Grant KE, Anbar AD (2024) Rhenium isotope reconnaissance of uranium ore concentrates, Earth Planet. Sci. Lett. DOI 10.1016/j.epsl.2024.118898

[16] Shollenberger QR, Borg LE, Ramon EC, Sharp MA, Brennecka GA (2021) Samarium isotope compositions of uranium ore concentrates: A novel nuclear forensic signature, Talanta DOI 10.1016/j.talanta.2020.121431

[17] Mughabghab SF (2003) The thermal neutron capture cross sections resonance integrals and g-factors, in: INDC (NDS)-440, International Atomic Energy Agency 1–31

[18] Mass R, McCulloch MT (1990) A search for fossil nuclear reactors in the Alligator River Uranium Field, Australia: Constraints from Sm, Gd, and Nd isotopic studies, Chem. Geol. DOI 10.1016/0009-2541(90)90095-O

[19] Hidaka H, Gauthier-Lafaye F (2001) Neutron capture effects on Sm and Gd isotopes in uraninites, Geochim. Cosmochim. Acta DOI 10.1016/S0016-7037(00)00567-6

[20] Hidaka H, Ebihara M, Yoneda S (1999) High fluences of neutrons determined from Sm and Gd isotopic compositions in aubrites, Earth Planet. Sci. Lett. DOI 10.1016/S0012-821X(99)00221-6

[21] Hidaka H, Kondo T, Yoneda S (2012) Heterogeneous isotopic anomalies of Sm and Gd in the Norton county meteorite: evidence for irradiation from the active early sun, ApJ DOI 10.1088/0004-637X/746/2/132

[22] Hidaka H, Ebihara M (1995) Determination of the isotopic compositions of samarium and gadolinium by thermal ionization mass spectrometry, Anal Chem 1437-1441

[23] Mizutani Y, Hidaka H, Yoneda S (2020) Chemical separation and determination of the isotopic compositions of dysprosium, erbium and ytterbirum in geochemical materials by thermal ionization mass spectrometry, Geochem. J. DOI 10.2343/geochemj.2.0609

[24] Isnard H, Brennetot R, Caussignac C, Caussignac N, Chartier F (2005) Investigations for determination of Gd and Sm isotopic compositions in spent nuclear fuel samples by MC-ICPMS, Int. J. Mass Spectrom. 246: 66-73

[25] Saji NS, Wielandt D, Paton C, Bizzarro M (2016) Ultra-high-precision Nd-isotope measurements of geological materials by MC-ICPMS, J. Anal. At. Spectrom., 31: 1490

[26] Yokoyama T, Fukai R, Nakahara M (2020) Separation of heavy lanthanoids by flash column chromatrography for precise determination of Er and Yb isotope compositions in rock samples, Geostand. Geoanalytical Res. 44: 265-285

[27] Frossard P, Ball JMJ, Schönbächler M (2025) High-precision Sm isotope analysis by thermal ionization mass spectrometry for large meteorite samples (>1g), J. Anal. At. Spectrom., 40: 146

[28] Fujii T, Moynier F, Albarede F (2009) The nuclear field shift effect in chemical exchange reactions, Chem. Geol. DOI 10.1016/j.chemgeo.2009.06.015

[29] Moynier F, Fujii T, Brennecka GA, Nielsen SG (2013) Nuclear field shift in natural environments, C R Geosci. DOI 10.1016/j.crte.2013.01.004

[30] Hidaka H, Yoneda S (2007) Sm and Gd isotopic shifts of Apollo 16 and 17 drill stem samples and their implications for regolith history, Geochim. Cosmochim. Acta DOI 10.1016/j.gca.2006.10.015

[31] Hidaka H, Sakuma K, Nishiizumi K, Yoneda S (2017) Isotopic evidence for multi-stage cosmic-ray exposure histories of lunar meteorites: long residence on the moon and short transition to the Earth, AJ DOI 10.3847/1538-3881/aa7139

[32] Kirchenbaur M, Maas R, Ehrig K, Kamenetsky VS, Strub E, Ballhaus C, Münker C (2016) Uranium and Sm isotope studies of the supergiant Olympic Dam Cu-Au-U-Ag deposit, South Australia, Earth Planet. Sci. Lett. DOI 10.1016/j.gca.2016.01.035

[33] DeLaeter JR, Rosman KJR, Smith CL (1980) The Oklo natural reactor: cumulative fission yields and retentivity of the symmetric mass region fission products. Earth Planet. Sci. Lett. 50: 238-246

[34] Gauthier-Lafaye F, Holliger P, Blanc PL (1996) Natural fission reactors in the Franceville basin, Gabon: a review of the conditions and results of a “critical event” in a geologic system, Geochim. Cosmochim. Acta 60: 4831-4852

[35] Hidaka H, Holliger P (1998) Geochemical and neutronic characteristics of the natural fossil fission reactors at Oklo and Bangombe, Gabon, Geochim. Cosmochim. Acta 62: 89-108

[36] Lingenfelter RE, Canfield EH, Hampel VE (1972) The lunar neutron flux revisited*, Earth Planet. Sci. Lett. 16: 355-369